Article

Martian Regolith Simulant-Based Geopolymers with Lithium Hydroxide Alkaline Activator

Jasper Vitse [1], Jiabin Li [1], Luc Boehme [1], Rudy Briers [2] and Veerle Vandeginste [3],*

[1] Department of Civil Engineering, Building Materials and Constructions, KU Leuven Campus Bruges, B-8200 Bruges, Belgium; jasper.vitse@kuleuven.be (J.V.); jiabin.li@kuleuven.be (J.L.); luc.boehme@kuleuven.be (L.B.)

[2] Department of Education, Core Research and Engineering, KU Leuven Campus Bruges, B-8200 Bruges, Belgium; rudy.briers@kuleuven.be

[3] Department of Materials Engineering, Surface and Interface Engineered Materials, KU Leuven Campus Bruges, B-8200 Bruges, Belgium

* Correspondence: veerle.vandeginste@kuleuven.be

Abstract: As humanity envisions the possibility of inhabiting Mars in the future, the imperative for survival in the face of its challenging conditions necessitates the construction of protective shelters to mitigate the effects of radiation exposure and the absence of atmospheric pressure. The feasibility of producing geopolymers using the Martian regolith simulant MGS-1 (as precursor) for potential building and infrastructure projects on Mars in the future is investigated in this paper. Various alkaline activators, such as sodium hydroxide (NaOH), lithium hydroxide ($LiOH \cdot H_2O$) and sodium silicate (Na_2SiO_3), are employed to investigate their efficiency in activating the precursor. The influence of alkali type and concentration on the mechanical performance of the synthesized geopolymers is examined. Geopolymer samples are oven-cured for 7 days at 70 °C before a compressive strength test. It is found that through the hybrid use of $LiOH \cdot H_2O$ and NaOH with optimal concentrations, metakaolin and milled MGS-1 as precursors, geopolymer mixtures with a compressive strength of 30 ± 2 MPa can be developed. The present test results preliminarily demonstrate the potential of Martian regolith simulant-based geopolymers as suitable construction and building materials for use on Mars.

Keywords: geopolymer; Mars; lithium hydroxide; compressive strength; cosmic radiation protection

1. Introduction

Beyond Earth, Mars seems to offer the best potential so far for humans to live since water has been found on this planet, and other conditions, such as temperature, are more suitable than on other planets [1]. Counted from the sun, Mars holds the fourth position in our solar system, orbiting between Earth and Jupiter. The red planet has an average atmospheric pressure of only 0.6% of that of the Earth [2]. Mars' atmosphere is largely made up of carbon dioxide, accounting for 95.3% of its total volume [3]. Nevertheless, with the Mars Oxygen In Situ Resource Utilization Experiment (MOXIE) technology, Marsrover Perseverance recently successfully produced oxygen from carbon dioxide in the Martian atmosphere through the use of solid oxide electrolysis. In the MOXIE technology, the Martian carbon dioxide is heated to around 800 °C, which separates oxygen and simultaneously generates carbon monoxide as a byproduct [4].

These recent technical innovations and findings indicate the potential to generate oxygen and eventually realize another most basic need for human life on Mars [5]. To shield the oxygen from the carbon-rich atmosphere on Mars, it has to be produced in a sheltered space which is not in direct contact with the Martian atmosphere [6,7]. Furthermore, buildings and infrastructure are also needed for humans to live on Mars. To develop civil engineering projects, building materials are necessary. In the selection of building

materials, the extreme environmental conditions on Mars must be taken into account. The cosmic radiation on Mars is reported to be 13 times higher than that on Earth, making it a challenging issue to solve [8]. Another challenge is related to the temperature on Mars [9]. The average surface temperature of Mars is $-63\,°C$, with a maximum daily temperature difference of $60\,°C$ [10].

Beyond the requirement for these building materials to withstand the severe environmental conditions on Mars, another concern arises [11]. The long distance between Earth and Mars, which varies from 54.6 to 401 million kilometers due to the different orbits of the two planets, and the high transportation cost [12] would make it very expensive to transport all the required raw materials from Earth to Mars. Therefore, it is more appropriate to use building materials in situ or to produce building materials with locally available raw resources on Mars. In this regard, whether the local raw materials and the resulting building materials and products are able to meet the technical requirements represents the most important question.

Binding materials (or binders) are frequently employed in building and infrastructure projects, which glue granular or bulk materials together as a whole. Cement is a typical binder with very popular use in the construction industry. The main issue related to cement is its production process, which is energy-intensive and emits a significant amount of CO_2, thus resulting in a negative environmental impact [13]. Geopolymers are a type of alternative binder to ordinary Portland cement, which, unlike the latter, are manufactured through the activation of aluminosilicate powders through use of alkaline solutions [14–16]. In comparison to ordinary Portland cement, geopolymers generally have a lower environmental impact while exhibiting similar or even better mechanical and durability performance [17].

Besides water, aluminosilicate-rich materials are also found on Mars [1], indicating the possibility of producing geopolymers there. Moreover, the available water can be used to optimize the workability of these geopolymers. In previous studies, some efforts have been made to explore the potential of using local sources on Mars to develop geopolymers. Alexiadis et al. (2017) and Chakraborty (2019) investigated the geopolymerization of JSC MARS-1A and MMS-1 Martian simulants using a combination of NaOH and Na_2SiO_3 as alkaline activators. The synthesized geopolymers exhibited a maximum compressive strength of 18.4 ± 1.6 MPa after curing in an oven at $80\,°C$ for 28 days and 5.0 ± 0.3 MPa after oven curing at $90\,°C$ for 7 days, respectively [18,19]. Ma et al. (2022) studied the printability and strength properties of 3D-printed Martian regolith-based geopolymer composites [20]. The compressive strength of the 3D-printed Martian regolith HIT-MRS-1 reinforced with basalt fibers was only 9.3 ± 0.8 MPa for suture pattern printing at $25\,°C$ after 10 days of ambient curing. Those very low strength values of the geopolymers are mainly due to shrinkage cracking and obviously limit, to a great extent, their implementation in practical projects. Further research is thus needed.

The objective of this study is to investigate the possibility of using aluminosilicate sources available on Mars to develop geopolymers with adequate technical properties as construction and building materials, especially for structural purposes. In the present work, the Mars Global Simulant MGS-1 is used, a regolith simulant for the Gale Crater on Mars [21]. Lithium hydroxide ($LiOH·H_2O$) is used as an alkaline activator since it can offer excellent resistance to the high-energy galactic cosmic rays on Mars [22,23]. A further optimization is made based on previous results with sodium silicate and lithium hydroxide [24]. The use of lithium hydroxide as an alkaline activator for producing geopolymers with Martian regolith is investigated here for the first time, representing the significant novelty of this work. It should be noted that lithium is available on Mars, which is generated due to the high rate of cosmic ray arrival [25]. A few previous studies have reported the use of lithium hydroxide as an alkaline activator to develop geopolymers with other types of precursors. For instance, Chen et al. (2012) studied the geopolymerization of brick powders with lithium hydroxide as an alkaline activator and achieved compressive strength values of up to 28 MPa [26]. Askarian et al. (2019) reported fly-ash-based geopolymers with a

28-day compressive strength of 22.6 MPa with the combined use of lithium hydroxide, calcium hydroxide and sodium silicate as alkaline activators [24].

However, so far, no research on the development of geopolymers with Martian simulants as precursors and lithium hydroxide as an alkaline activator has been reported in the literature. This research aims to evaluate the feasibility of making geopolymers with sufficient strength from the Martian simulant MGS-1 by preparing and testing a series of geopolymer mixtures. Therefore, the research objectives are as follows:

(1) To examine the influence of the alkaline solution type and concentration on the compressive strength performance of Martian regolith-based geopolymers.
(2) To gain insight into the strength–microstructure relations through FTIR, XRD and SEM analyses of the Martian regolith-based geopolymer samples.

2. Materials and Methods

2.1. Geopolymer Precursors

Mars Global Simulant (MGS-1) and metakaolin (MK) were used as precursors to prepare the geopolymers. A visual representation of the two precursors is shown in Figure 1a,b. The chemical compositions of the precursors determined through X-ray fluorescence (XRF, Bruker S8 TIGER wavelength-dispersive spectrometer) spectrometry are illustrated in Table 1. These results indicate that MGS-1 is very rich in SiO_2 (50.8 wt%) and consists, to a lesser extent, of Al_2O_3 (8.9 wt%) and CaO (3.7 wt%). The chemical composition of metakaolin ($Al_2O_3 \cdot 2SiO_2$) confirms the beneficial high amount of SiO_2 (53.4 wt%) and Al_2O_3 (44.5 wt%) for geopolymerization, compared to that of MGS-1.

| (a) | (b) |

Figure 1. Geopolymer precursors: (**a**) MGS-1 after 6 h of milling with a Bottle Roller and (**b**) metakaolin after the calcination of kaolinite for 3 h at 650 °C.

Table 1. Chemical compositions of Martian regolith MGS-1 and metakaolin (wt%).

Precursor	SiO_2	TiO_2	Al_2O_3	Cr_2O_3	FeO_T	MnO
MGS-1	50.8	0.3	8.9	0.1	13.3	0.1
MK	53.4	0.8	44.5	0.1	0.4	0.1
Precursor	**MgO**	**CaO**	**Na_2O**	**K_2O**	**P_2O_5**	**SiO_3**
MGS-1	16.7	3.7	3.4	0.2	0.4	2.1
MK	0.1	0.1	0.2	0.1	0.1	0.1

During geopolymerization, the SiO_4 and AlO_4 tetrahedra in the metakaolin structure will react with our alkaline activator components, which are a combination of sodium and lithium hydroxide, to form polymeric Si-O-Al bonds, leading to the formation of a three-dimensional network structure of geopolymers with enhanced density and strength [27].

2.2. Alkaline Activators

Sodium hydroxide (NaOH, 99% purity pellets), lithium hydroxide (LiOH·H_2O, 98% purity flakes) and sodium silicate (Na_2SO_3) solution (25.9 wt% SiO_2, 7.9 wt% Na_2O and 66.2 wt% H_2O) were used as alkaline activators. Deionized water was used for the dissolution of the solid sodium hydroxide pellets and lithium hydroxide flakes.

2.3. Geopolymer Raw Material Preparation

To increase the specific surface area of the Martian simulant used, i.e., MGS-1, the original material with an average grain size of 122 μm was ground using a Laarmann LMBR500 Bottle Roller (Figure 2a) at a speed of 225 rpm for 6 h [28,29]. The employed metakaolin was produced by means of the calcination of the clay mineral kaolinite in a furnace (Figure 2b) at 650 °C for 180 min, in accordance with former studies [30,31]. The MGS-1 and metakaolin precursors were first blended and mixed for 2 min at a speed of 140 rpm into a homogeneous mixture.

(**a**) Grinding equipment (**b**) Furnace

Figure 2. Precursor preparation equipment for grinding and calcination.

The solid NaOH pellets were mixed with deionized water and stirred to complete dissolution. The LiOH·H_2O flakes were then added to the NaOH solution (Figure 3a), and the exothermic reaction of NaOH dissolution, causing an increase in the temperature of the solution, was able to accelerate the dissolution process of the flakes. After that, the alkaline solution with NaOH and LiOH·H_2O was ambient-air-cooled for 24 h [32]. Finally, the obtained solution was blended with the Na_2SiO_3 solution (Figure 3b) and stirred for 3 min to reach a uniform mixture, followed by cooling to ambient temperature.
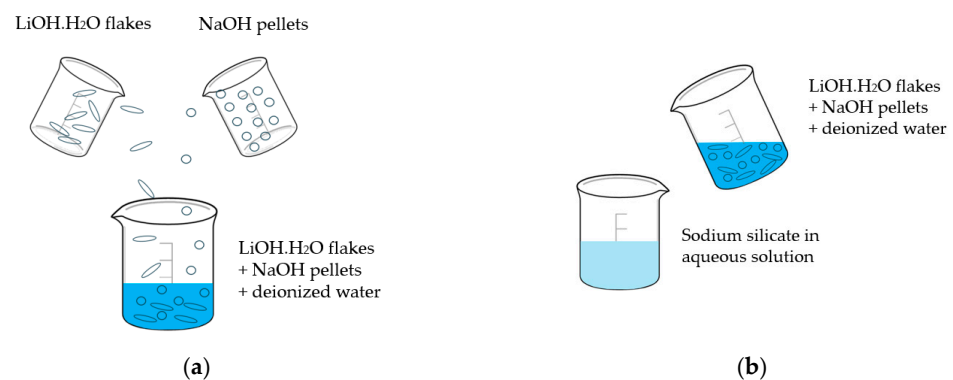

(**a**) (**b**)

Figure 3. Alkaline activator preparation: (**a**) blending LiOH·H_2O and NaOH with deionized water and (**b**) stirring hydroxide mixture with sodium silicate solution for 3 min.

2.4. Geopolymer Mixtures

Different geopolymer compositions were made by varying the alkaline activator LiOH·H₂O concentration from 6 M to 8 M, based on previous studies on the geopolymerization of other types of Martian simulants [18,19,33]. Table 2 gives an overview of all compositions made in this work. Table 3 illustrates the mixtures of geopolymers according to the aluminosilicate precursors and alkaline activators.

Table 2. Alkaline activators and their molar ratios in alkaline solution.

No.	Alkali Hydroxide Activators	Molar Ratios in Alkaline Solution	
		SiO₂/Na₂O	SiO₂/Li₂O
1	8 M NaOH	0.242	-
2	6 M LiOH·H₂O + 1 M NaOH	0.718	0.425
3	8 M LiOH·H₂O + 1 M NaOH		0.319
4	6 M LiOH·H₂O + 0.5 M NaOH	0.836	0.425
5	8 M LiOH·H₂O + 0.5 M NaOH		0.319
6	6 M LiOH·H₂O + 1.5 M NaOH	0.630	0.425
7	8 M LiOH·H₂O + 1.5 M NaOH		0.319

Table 3. Geopolymer mixture design for 100 mL of geopolymer, in grams.

Geopolymer Mixture	MGS-1 (Milled)	Metakaolin	NaOH Pellets	LiOH·H₂O Flakes	Na₂SiO₃ Solution	Water [a]
1	72.2	36.7	9.6	-	34.2	11.6
2	72.2	36.7	5	7.6	33.5	11.3
3	72.2	36.7	5	10.1	31.3	10.6
4	72.2	36.7	2.5	7.6	33.5	11.3
5	72.2	36.7	2.5	10.1	31.3	10.6
6	72.2	36.7	7.5	7.6	33.5	11.3
7	72.2	36.7	7.5	10.1	31.3	10.6

[a] Water amount used for dissolving LiOH·H₂O flakes and/or NaOH pellets.

2.5. Geopolymer Synthesis and Production

An important factor for the mix design of geopolymers is the ratio of alkaline solution to solid aluminosilicates. Montes et al. (2015) found that the optimal alkaline activator/aluminosilicate mass ratio is 0.32 for geopolymers with the simulated lunar regolith Lun-Cast-3D as a precursor [33]. For the geopolymerization of MGS-1 in this study, the alkaline solution/aluminosilicate volume ratio was fixed at 0.30 for all seven mixtures. Due to the high cost of the alkaline activator, the lowest amount of activator was used, resulting in a volume ratio of 0.3. Furthermore, the volume ratio of the amount of metakaolin to MGS-1 was empirically fixed at 0.20 since the Al/Si atomic ratio for the solid precursors was fixed at 1.0 in this work [34].

In preparing the geopolymer pastes, the solid precursors MGS-1 and metakaolin were first mixed with an electric blender at a rate of 140 rpm for 2 min until a homogeneous mix was reached. Then, the Na₂SiO₃ solution was added to the precursors, followed by mixing for 3 min (per 200 mL of geopolymer mixture). Figure 4 shows a flowchart for the preparation of the geopolymers in this work [35].
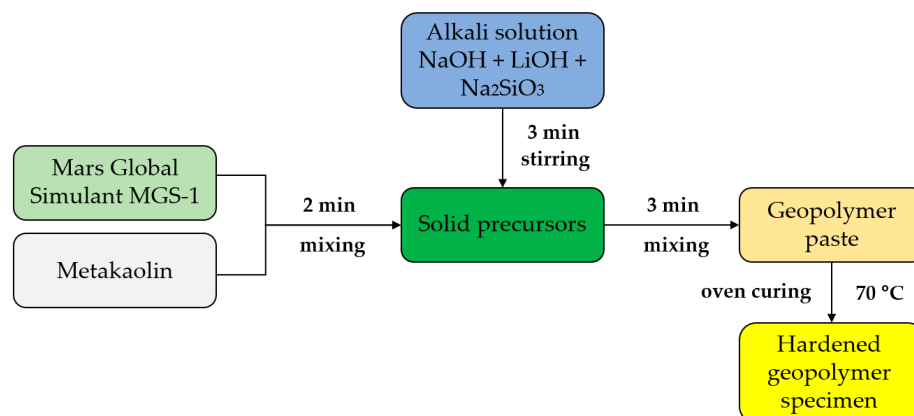
Figure 4. Flowchart of geopolymer production.

The freshly mixed geopolymer pastes were cast into cylindrical molds of Ø 20 × 40 mm. The geopolymer pastes were then compacted through the use of a modified, custom-made pellet press, as shown in Figure 5a. This device compacted the geopolymer into 4 equal 10 mm-heigh layers of a cylindrical sample, each time with an imposed compressive force of 250 kg or a compressive pressure of 7.81 MPa. Through the use of this pellet press, the compaction degree of the geopolymers can easily be controlled. The geopolymers consist of a total of 7 different chemical compositions (as shown in Table 2), with 6 cylindrical samples per mixture. Figure 5b shows a typical cylindrical geopolymer sample.

(**a**) pellet press (**b**) Cylindrical geopolymer sample (length = 40 mm; diameter = 20 mm)

Figure 5. Geopolymer production equipment and geopolymer samples.

2.6. Curing

All geopolymer pastes were oven-cured for 1 d, 3 d, 7 d or 28 d at a constant temperature of 70 °C. A temperature of 70 °C is commonly employed for the curing of geopolymers since metakaolin-based geopolymers gain the highest mechanical strength when cured in an oven at a temperature between 60 °C and 80 °C [36]. In this paper, the evolution of the compressive strength was studied after 1 d, 3 d, 7 d and 28 d of curing in the oven at 70 °C for geopolymer mixtures 1, 2 and 3. For geopolymer mixtures 4–7, compressive strength tests were performed after 1 d, 3 d and 7 d of oven curing at 70 °C.

2.7. Particle Size Distribution Analysis of Precursors

The grinding and calcination effects of Martian regolith MGS-1 and kaolinite, respectively, on the particle size distribution were analyzed with a Fritsch Dry Dispersion Unit Laser Analysette 22, as shown in Figure 6a. This laser granulometer is equipped with advanced optics and a robust laser system, ensuring high measurement sensitivity and accuracy. The instrument covers a broad measurement range, between 0.3 and 300 µm. A total of six measurements were performed for each sample, where the curved line represents the cumulative particle size distribution. Before the measurements, both precursors were stored in a furnace at 110 °C for 24 h to guarantee that the samples were completely oven-dry.

(**a**) particle size analysis of geopolymer precursors   (**b**) compressive strength testing

Figure 6. Particle size analysis and compressive strength testing of geopolymer samples.

2.8. Characterization of Geopolymers

A Perkin Elmer (Waltham, MA, USA) UATR Two Fourier Transform Infrared Spectrometer (FT-IR Perkin Elmer Model 100 spectrometer equipped with an attenuated total reflectance of 125 accessories) was used to characterize the functional groups of the manufactured geopolymers based on vibrational energy [37]. The FTIR spectra were recorded in the range between 400 and 4000 cm^{-1}, with a resolution of 2 cm^{-1}. Each mixture that was subjected to a compression test was also analyzed by FTIR. This was carried out on geopolymer specimens finely ground into powders after the compression test. Scanning electron microscopy (SEM) was used to investigate the surface topography and porosity of the geopolymer mixtures. These characteristics can be used to examine the correlation between the porosity and compressive strength of the geopolymers. X-ray diffraction (XRD) analysis was employed to determine the mineralogical composition and crystallographic structure of the geopolymers. The XRD spectra of the geopolymer mixtures were recorded between 5 and 65° 2θ on a Bruker D2 PHASER machine, with a step size of 0.02° 2θ and a scan rate of 1°/min, using a Cu Kα X-ray source (λ = 1.542 Å).

2.9. Compressive Strength

A semi-automatic compressive testing machine (MATEST, Treviolo, Italy), as shown in Figure 6b, was used to measure the compressive strength of the manufactured geopolymer samples, as per EN-196-1 [38]. The compressive strength results are presented as the mean value, μ, from the test dataset measured on six specimens, with the standard deviation, σ. In this paper, the compressive strength, f_c, is thus denoted as $f_c = \mu + \sigma$. Outliers were

removed from the dataset in order to obtain more representative values for the compressive strength. Prediction intervals were used to detect whether a measurement was an outlier, since it often cannot be simply assumed that the measured values follow a Gaussian distribution. The scientific background for a prediction interval is the t-distribution, which is a derivative of the Gaussian distribution [39]. Therefore, the use of prediction intervals is a more objective way of making judgments about outliers from randomly distributed data. The significance level for the maximum allowed errors on the measured data was assumed to be 5%, with a minimum of 10 data elements for the t-distribution.

3. Results

3.1. Grinding and Calcination Effects on Particle Size Distribution of Precursors

3.1.1. Grinding Effect of MGS-1

The effect of grinding the Martian regolith MGS-1 for 6 h through the use of the Laarmann LMBR500 Bottle Roller on the particle size distribution is shown in Figure 7. Both relative and cumulative distributions before (black) and after grinding (grey) are presented. From the obtained particle size distributions after grinding MGS-1, a decrease in the overall average particle size, D_{50}, from 122 µm to 5 µm was observed.
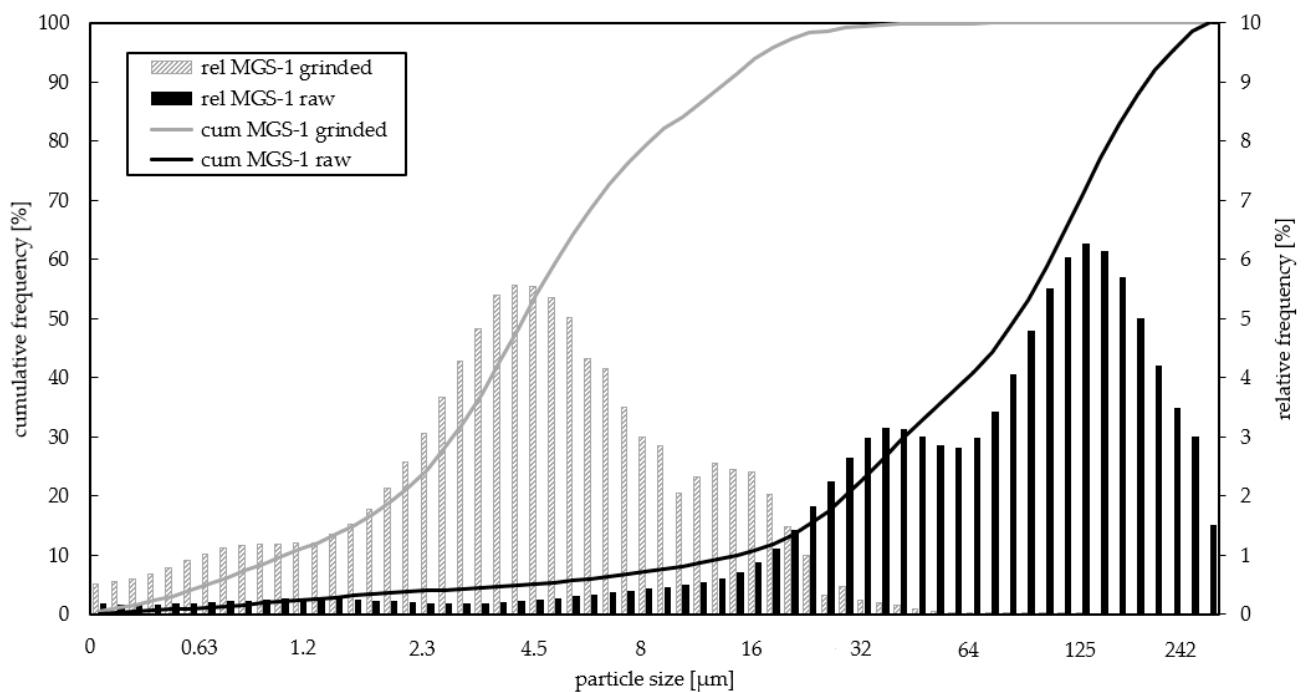

Figure 7. Grinding's effect on the particle size distribution of MGS-1 before grinding (black) and after 6 h of grinding at 225 rpm (grey).

3.1.2. Calcination Effect of Kaolinite

The effect of the calcination of kaolinite for 3 h at 650 °C on the particle size distribution is shown in Figure 8. The process of calcinating kaolinite into metakaolin also impacted the particle size distribution. A slight reduction in the average particle size, D_{50}, can be observed, from 7 µm (kaolinite) to 1.7 µm (metakaolin) after calcination.
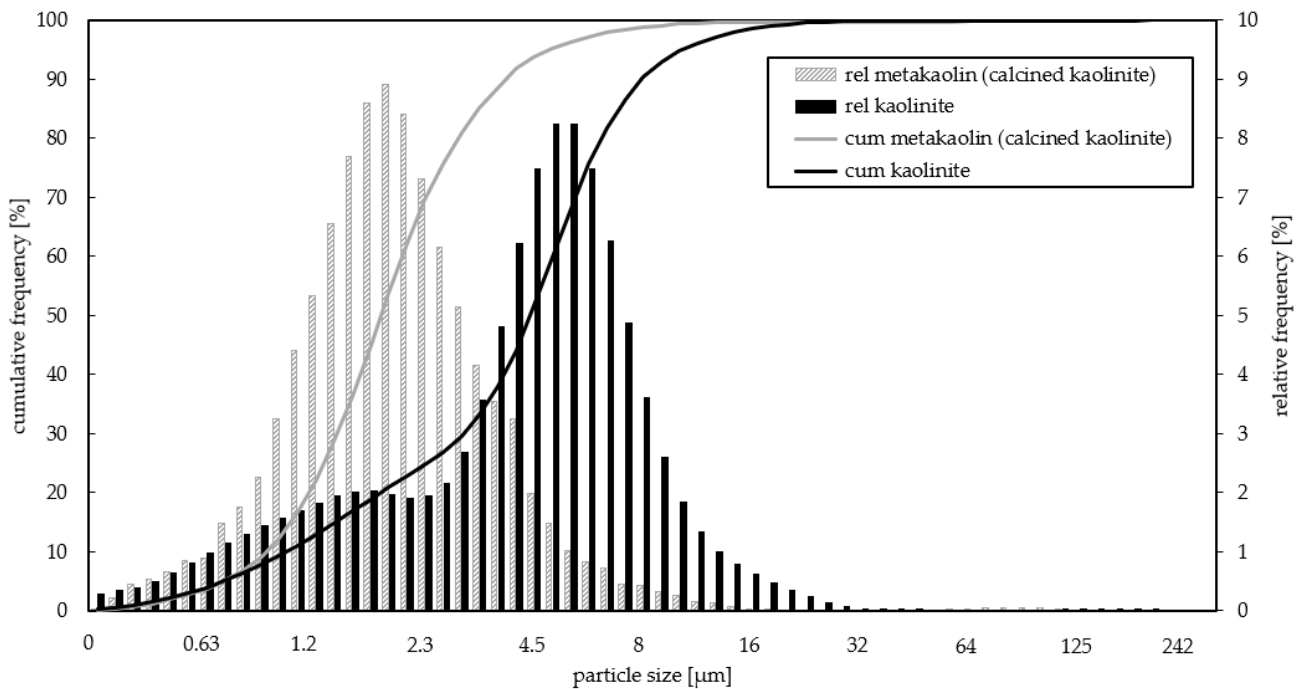
Figure 8. Calcination's effect on the particle size distribution of the kaolinite precursor before the calcination of kaolinite (black) and after 3 h of calcination at 650 °C of metakaolin (grey).

3.2. Compressive Strength

Figure 9a presents the measured compressive strength values of geopolymer mixtures 1–3 at various ages, i.e., 1 d, 3 d, 7 d and 28 d. The figure shows that the compressive strength of mixture 1 consecutively increased with curing age within the investigated range. At a curing age of 28 d, a compressive strength of 5.8 ± 2.9 MPa was achieved. In comparison to geopolymer 1, mixtures 2 and 3 exhibited significantly higher compressive strengths, irrespective of the testing age.
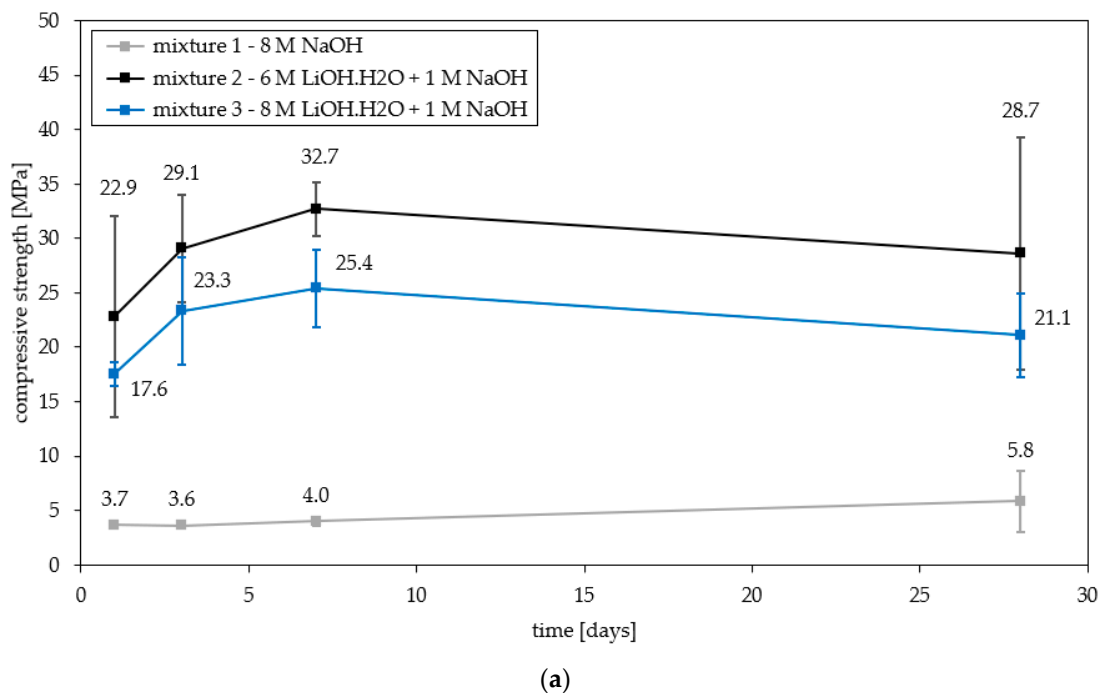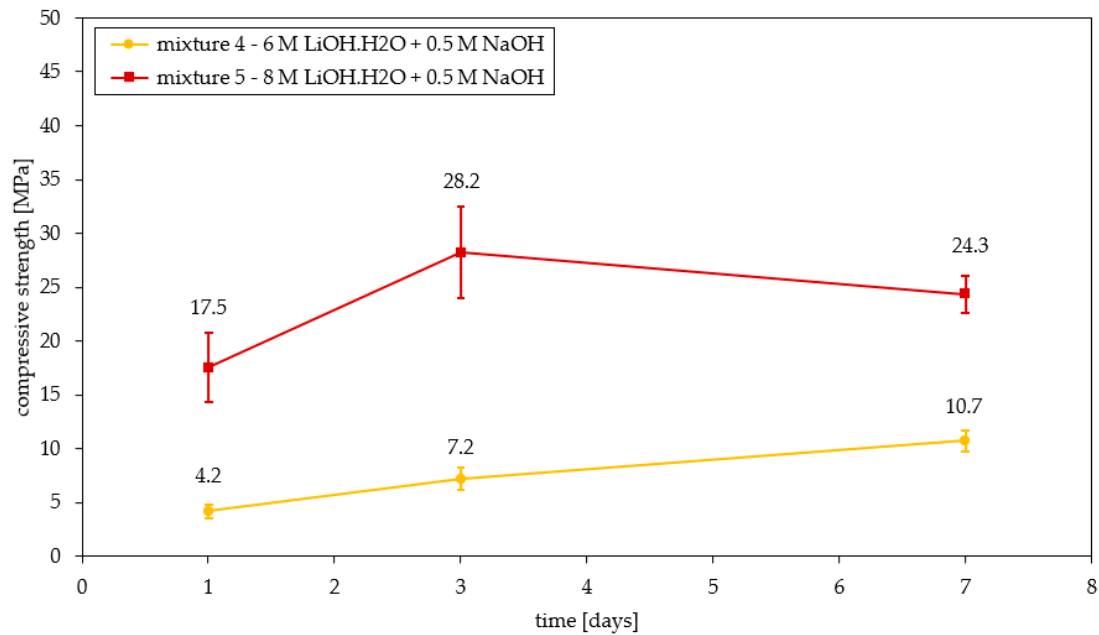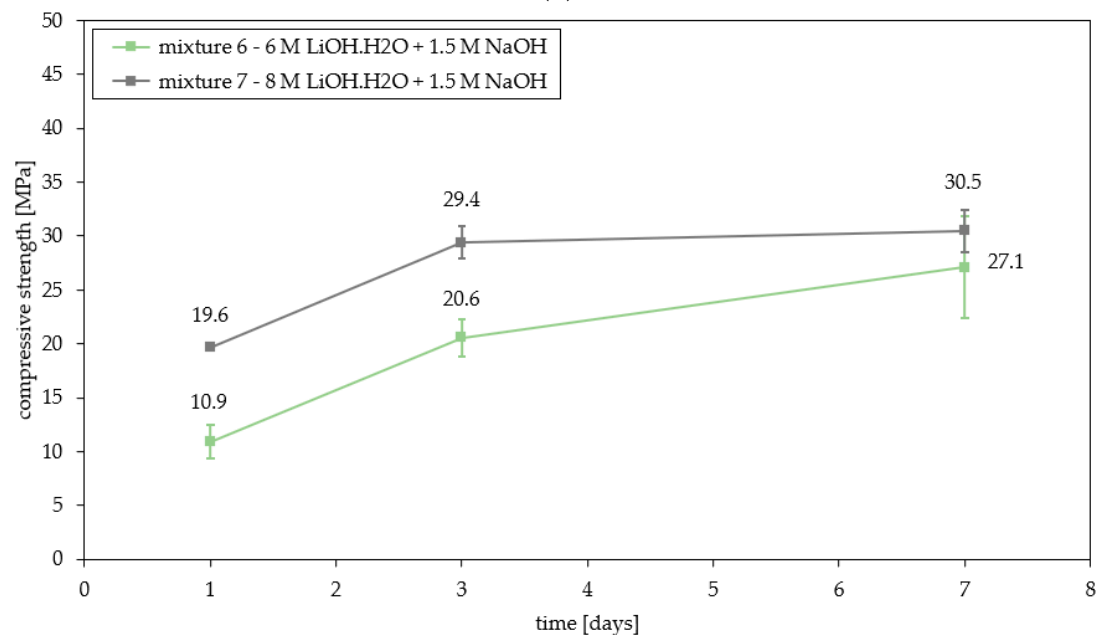

(a)

Figure 9. *Cont.*

(**b**)

(**c**)

Figure 9. Measured compressive strengths of geopolymers: (**a**) mixtures 1–3; (**b**) mixtures 4–5; and (**c**) mixtures 6–7.

The measured compressive strength values of geopolymer mixtures 4 to 7, as shown in Figure 9b,c, indicate that when the NaOH concentration was 0.5 M and 1.5 M, an increase in the LiOH·H$_2$O concentration from 6 M to 8 M led to an increase in the compressive strength of the geopolymers within the investigated scope of this study.

3.3. FTIR Analysis

3.3.1. Precursors: MGS-1 and Metakaolin

The FTIR analyses of both geopolymer precursors, MGS-1 and metakaolin, are shown in Figure 10. Since the Martian simulant MGS-1 is an aluminosilicate, a similar strong peak to that of metakaolin is observed at a wavenumber of 1008 cm^{-1}. The absorption at this

wavenumber can be assigned to Si-O-Al asymmetric stretching vibrations within the TO_4 tetrahedra typical of amorphous aluminosilicates [40]. The adsorption band at 1623 cm^{-1} is attributed to the bending vibrations of H-O-H [41].
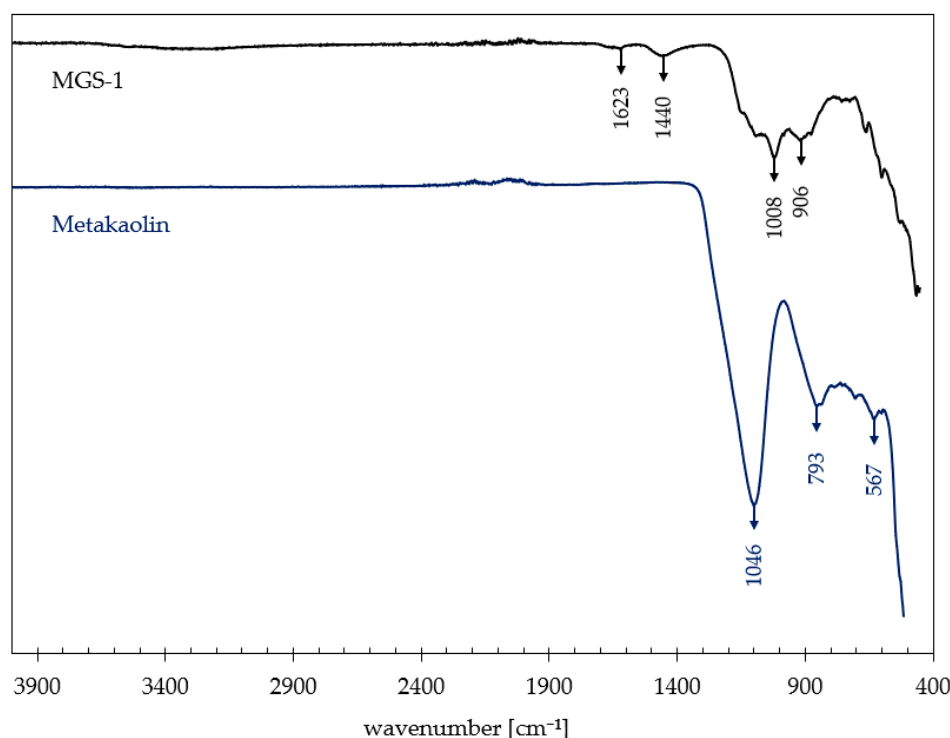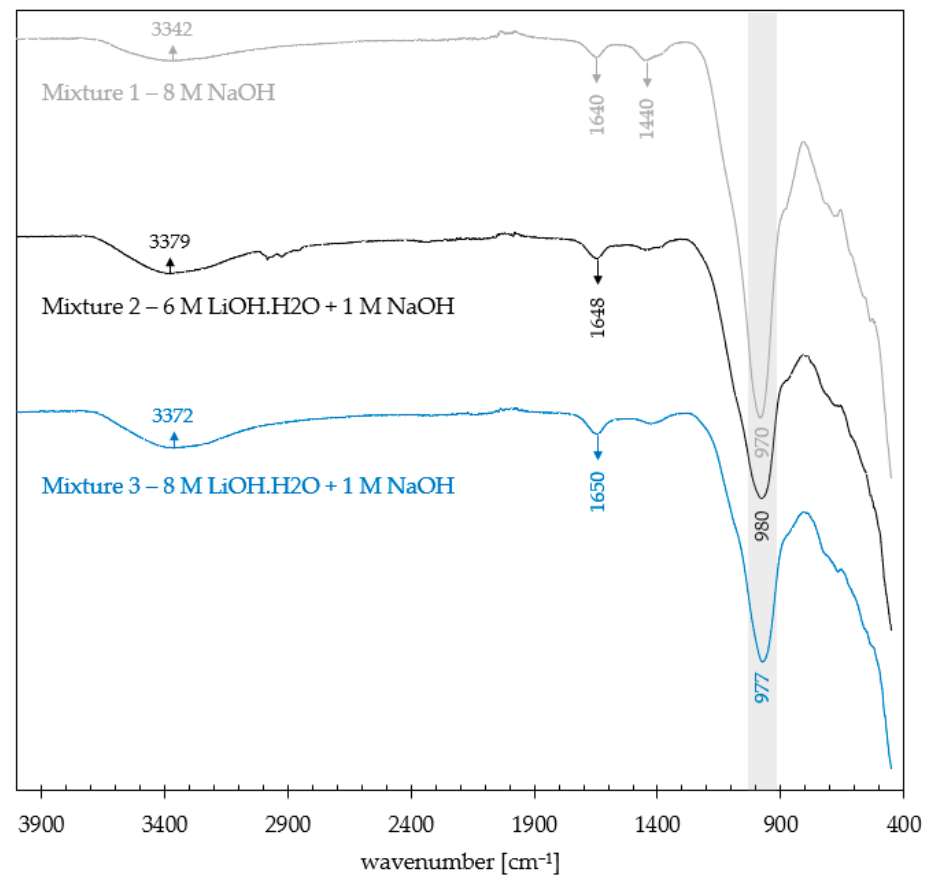

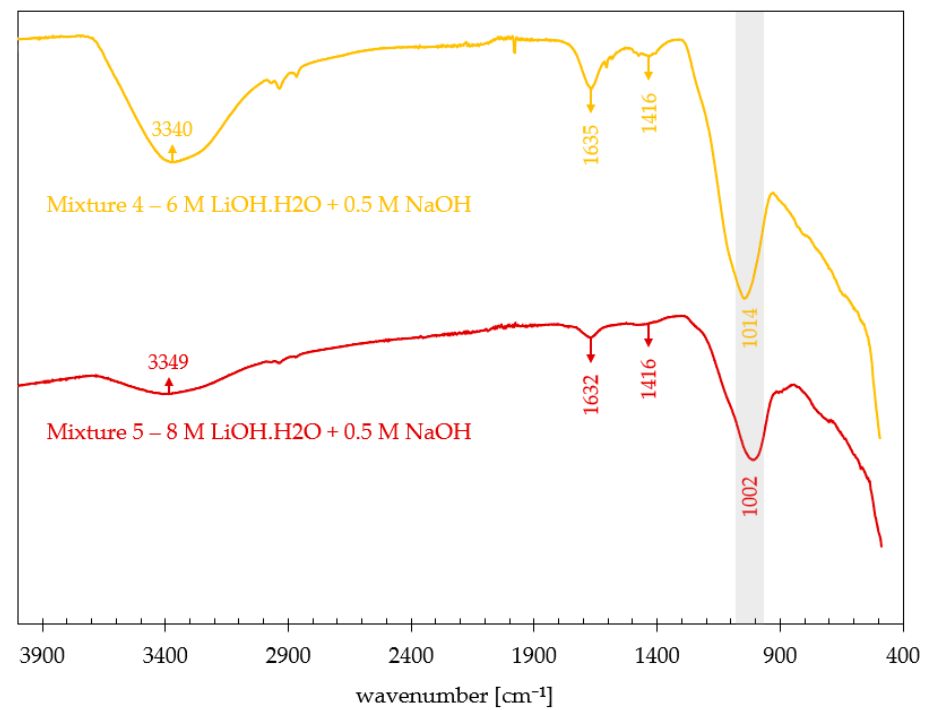**Figure 10.** FTIR spectra of geopolymer precursors MGS-1 and metakaolin.

The peak at a wavenumber of 1440 cm^{-1} indicates the carbonation phase. Finally, the peak at 906 cm^{-1} refers to the symmetric Si-O bonds. Small peaks are observed around 600 cm^{-1}, which imply the presence of silicates and aluminosilicate glasses in the Martian regolith simulant MGS-1 [42]. The FTIR spectra for metakaolin present three main peaks at wavenumbers 1046 cm^{-1}, 793 cm^{-1} and 567 cm^{-1}. The peaks observed below 900 cm^{-1} correspond to asymmetric vibrations of Si-O-(Si,Al), while those around 1050 cm^{-1} are associated with Si-O-Si bonds [43].

3.3.2. Geopolymer Mixtures

The FTIR analyses of all seven geopolymer mixtures are shown in Figure 11, where Figure 11a represents mixtures 1–3, Figure 11b represents mixtures 4–5 and Figure 11c represents mixtures 6–7. The measured FTIR spectrum of geopolymer mixture 1 shows four different peaks (Figure 11a). The broad absorption band at a wavenumber of 3342 cm^{-1} represents stretching vibrations of -OH groups and water molecules [44]. The peak at a wavenumber of 1640 cm^{-1} can be assigned to the bending vibrations of H-O-H, while 1440 cm^{-1} corresponds to C-O stretching vibrations from carbonate. Finally, the peak observed at a wavenumber of 970 cm^{-1} represents Si-O-Si asymmetric stretching vibrations [45].

(**a**)

(**b**)

Figure 11. *Cont.*
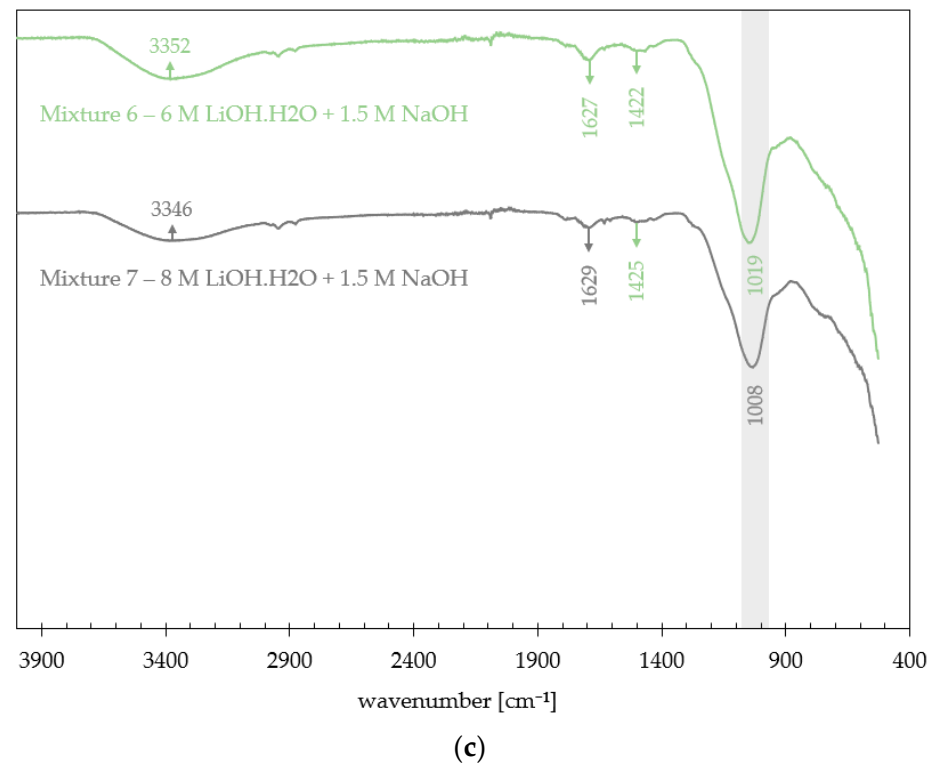
(c)

Figure 11. FTIR spectra of all seven geopolymer mixtures: (**a**) mixtures 1–3; (**b**) mixtures 4–5; (**c**) and mixtures 6–7.

In geopolymer mixtures 2 and 3, peaks are observed at wavenumbers 3372–3379 cm^{-1}, 1648–1650 cm^{-1} and 977–980 cm^{-1} (Figure 11a). These observed peaks are related to stretching vibrations of -OH groups and water molecules, bending vibrations of H-O-H and Si-O-T (T = Si or Al) asymmetric stretching vibrations, respectively [46]. Geopolymer mixtures 4 and 5 display strong peaks detected at wavenumbers of 3340–3349 cm^{-1}, 1632–1635 cm^{-1} and 1002–1014 cm^{-1} (Figure 11b). These peaks are related to stretching vibrations of -OH groups and water molecules, bending vibrations of H-O-H and Si-O-Si asymmetric stretching vibrations, respectively. The difference between the FTIR spectra of geopolymer mixtures 4 and 5 and geopolymer mixtures 6 and 7 is noticeable at the absorption band at 1416 cm^{-1} (Figure 11b). A clear peak at that wavenumber can be observed for geopolymer mixture 4. The peaks at wavenumbers of 3346–3352 cm^{-1} and 1627–1629 cm^{-1} in Figure 11c represent the vibration of -OH groups and water molecules, while the peak at wavenumber 1008–1019 cm^{-1} corresponds to Si-O-Si asymmetric stretching vibrations.

After geopolymerization, the characteristic band at 1050 cm^{-1} in metakaolin shifted towards lower frequencies, specifically at 970–980 cm^{-1}. This shift indicates a significant alternation in the chemical environment of both aluminum and silicon during the geopolymerization process [47]. The change in the chemical structure resulted in the generation of new substances with distinct chemical compositions compared to metakaolin.

3.4. Scanning Electron Microscope (SEM) Analysis

An SEM analysis was employed for the microstructural characterization of geopolymer mixtures 1–3 and 6–7. Due to high-resolution images and valuable information about the microstructure and morphology of the geopolymers, a relation between the pore structure and compressive strength can be drawn. The SEM image of geopolymer mixture 1, which had a relatively low compressive strength of 5.8 MPa after curing for 28 d, shows a porous structure with large pores in the geopolymer matrix (Figure 12a).
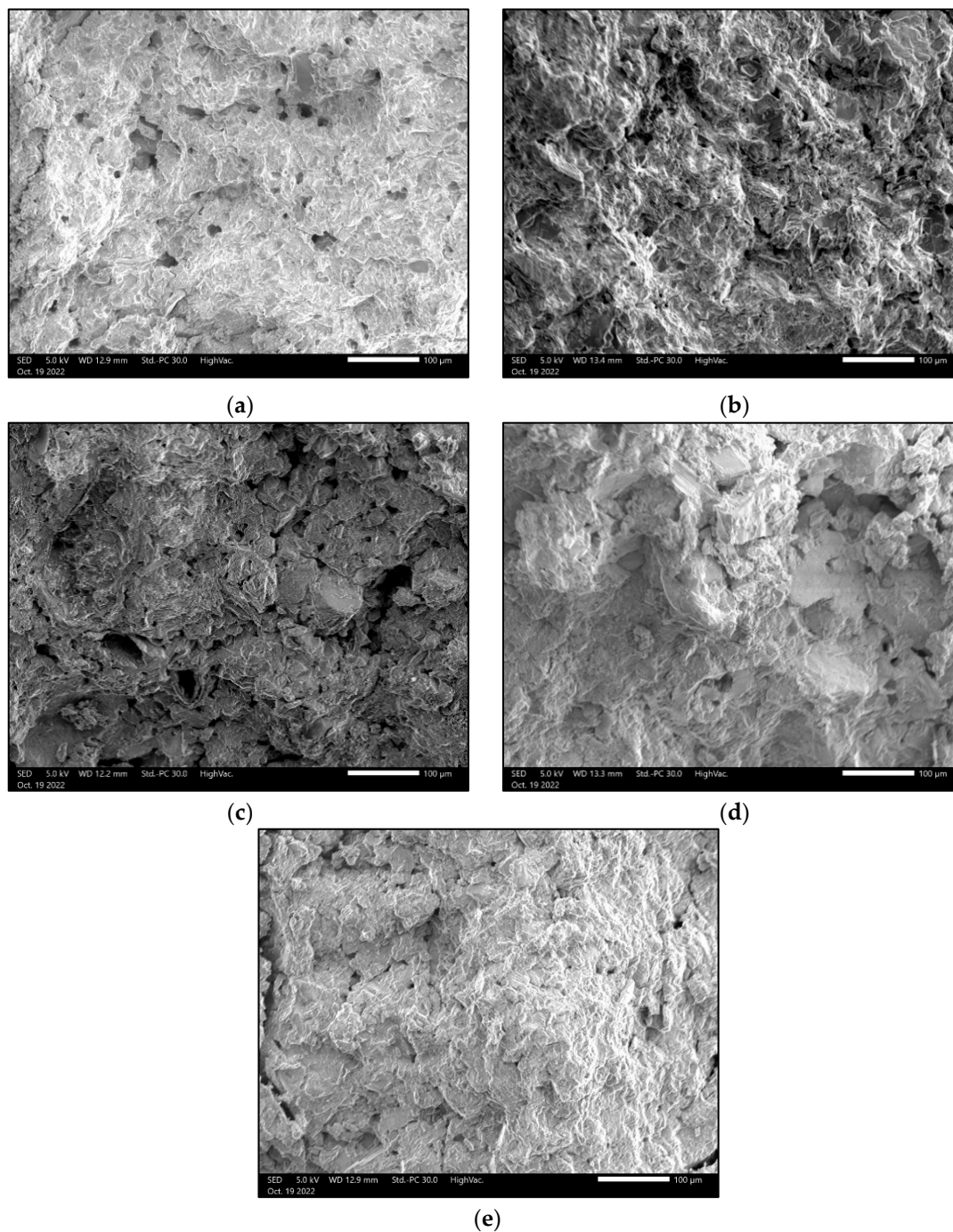
Figure 12. SEM images of geopolymers: (**a**) mixture 1; (**b**) mixture 2; (**c**) mixture 3; (**d**) mixture 6; and (**e**) mixture 7.

A comparison of the SEM images of geopolymer mixtures 2 and 3 indicates that geopolymer mixture 2 has a rougher surface but with fewer voids than mixture 3 (Figure 12b,c). The SEM images of geopolymer mixtures 6 and 7 reveal that these two mixtures have relatively dense structures with a limited number of large pores (Figure 12d,e). Geopolymer mixture 7 shows the highest density and the lowest tendency to pore formation (Figure 12e).

3.5. XRD Analysis

Figure 12 shows the X-ray diffraction data obtained from geopolymer mixtures 1–3 and 6–7. Through this analytical technique, the identification and characterization of crystalline materials in the geopolymer mixtures can be provided. The main crystalline phases (quartz,

forsterite, anorthite, calcite and pyroxene) in the geopolymer mixtures are indicated in the XRD data. A glassy, amorphous phase is present in all the samples, regardless of the combination of solids employed, within the 20–35° range of 2θ angles. This phenomenon is attributed to the development of an alkaline aluminosilicate gel, commonly referred to as the N-A-S-H gel, which serves as the primary product in the reaction pathway leading to the formation of geopolymers [48].

4. Discussion

4.1. Grinding and Calcination Effects on Particle Size Distribution of Precursors

The process of grinding involves reducing the size of particles through mechanical forces such as compression, impact, or attrition. Grinding MGS-1 breaks down larger particles, leading to an increase in the overall surface area. This results in more reactive sites on particle surfaces becoming accessible during the alkali activation process. Geopolymers derived from finely ground MGS-1 particles often exhibit improved mechanical properties [49]. The smaller particle sizes contribute to a denser and more compact microstructure, resulting in enhanced strength and durability for the geopolymer material [50].

The primary structural unit in kaolinite is a layer composed of one aluminum octahedral sheet and two silicon tetrahedral sheets. During calcination, kaolinite undergoes dehydration and dehydroxylation. Water molecules and hydroxyl groups are removed, leading to the collapse of the crystal structure [51]. Calcination disrupts the ordered crystalline structure of kaolinite, breaking down the large, stacked layers into smaller, more dispersed particles. The loss in crystallinity and the creation of a disordered structure contribute to the reduction in particle size [52].

4.2. Effects of Alkaline Solution Type and Concentration on Geopolymers' Compressive Strength

The observed variations in compressive strength among geopolymer mixtures 2 and 3 compared to mixture 1 can be attributed to the beneficial effects of $LiOH \cdot H_2O$ in the alkaline activator. However, the compressive strength of the samples is dependent on chemical parameters, more specifically, the concentration of $LiOH \cdot H_2O$. With an increase in the $LiOH \cdot H_2O$ concentration from 6 M to 8 M (with 1 M NaOH), the compressive strength of the geopolymers decreased, regardless of the curing time. For instance, the average 3 d compressive strength of geopolymer mixture 2 (6 M $LiOH \cdot H_2O$) was 29.1 MPa, while it was 23.3 MPa for geopolymer 3 (8 M $LiOH \cdot H_2O$). Until a curing age of 7 days, the measured compressive strength of both geopolymer mixtures increased with time. However, the 28 d compressive strength for both mixtures decreased in comparison to the 7 d strength. The reduction in compressive strength could have been caused by the long-term oven curing, which can increase the shrinkage-induced cracking tendency and impose a negative effect on the microstructure of the material. In terms of the 28 d compressive strength, geopolymer mixture 2 exhibited the highest value, with an average compressive strength of 28.7 MPa.

However, the influence of the $LiOH \cdot H_2O$ concentration used seems to be dependent on that of NaOH. The measured compressive strength values of geopolymer mixtures 4 to 7 indicate that when the NaOH concentration was 0.5 M and 1.5 M, an increase in the $LiOH \cdot H_2O$ concentration from 6 M to 8 M led to an increase in the compressive strength of the geopolymers within the investigated scope of this study. For instance, when the NaOH concentration was 0.5 M, geopolymer mixture 5 (with 8 M $LiOH \cdot H_2O$) reached an average compressive strength of 24.3 MPa at a curing age of 7 days, while mixture 4 (with 6 M $LiOH \cdot H_2O$) exhibited a 7 d compressive strength of 10.7 MPa. Similar results are also found for geopolymer mixtures 6 and 7, which had the same 1.5 M concentration of NaOH. However, in this case, the effect of the $LiOH \cdot H_2O$ concentration was less significant in comparison to that of geopolymers with 0.5 M and 1.0 M NaOH. Hence, it can be concluded that the influence of the $LiOH \cdot H_2O$ concentration on the compressive strength of the geopolymers with Martian simulant MGS-1 is dependent on the concentration of NaOH in the alkaline solutions. From the results in Figure 9b,c, a significant increase in compressive

strength was observed when the NaOH concentration in the 6 M LiOH·H$_2$O mixture was increased from 0.5 M to 1.5 M. For the 8 M LiOH·H$_2$O mixture, only a slight increase in compressive strength was observed when increasing the NaOH concentration from 0.5 M to 1.5 M. Soluble silica in sodium silicate can significantly shorten the time needed for the condensation of oligomers [53]. This results in an enhancement in the structural stability of the gels formed. Furthermore, a mix of NaOH and Na$_2$SiO$_3$ significantly improves the microstructure of the geopolymer framework. Specifically, Na$_2$SiO$_3$ addition allows for the formation of gel-like networks among the reacted/semi-reacted precursor particles, resulting in the fast growth of a structure in which particles are tightly wrapped and bridged. In other words, the interaction of the two alkaline activators has to be taken into account.

The effect of the NaOH concentration in the alkaline solution on the compressive strength of the Martian simulant MGS-1-based geopolymers can be examined by comparing the measured strength magnitudes of geopolymer mixtures 2, 4 and 6 as well as those of mixtures 3, 5 and 7. The test data indicate that when the LiOH·H$_2$O concentration is 6 M, an increase in the NaOH concentration in the alkaline solution from 0.5 M to 1.0 M and then to 1.5 M results first in an increase and then a decrease in the compressive strength of the geopolymers. For instance, the 7 d compressive strength of the geopolymers changed from 10.7 to 32.7 and then to 27.1 MPa when the NaOH concentration varied from 0.5 M to 1.0 M and then to 1.5 M. However, a different trend is observed when the concentration of LiOH·H$_2$O is 8 M in the alkaline solution. In this case, the increase in the concentration of NaOH in the alkaline solution generally yields an increase in the compressive strength of the geopolymers, as observed from the measured data on geopolymer mixtures 3, 5 and 7, which have a LiOH·H$_2$O concentration of 8 M. For example, when the NaOH concentration changed from 0.5 M to 1.0 M and then to 1.5 M in the alkaline solution, the 7 d compressive strength of the geopolymers increased from 24.3 to 25.4 and then to 30.4 MPa. It should be noted that the variation in the compressive strength is, in general, minor between geopolymer mixtures with 0.5 M and 1.0 M NaOH in the alkaline solution (when the LiOH·H$_2$O concentration is 8 M). The above analysis indicates that the influence of the concentration of LiOH·H$_2$O on the compressive strength of Martian simulant MGS-1-based geopolymers is dependent on the NaOH concentration in the alkaline solution, and vice versa. From the measured data, it is evident that geopolymer mixture 2 gives the highest 7 d compressive strength, which is 32.7 MPa (average value).

In previous work, Chen et al. (2012) investigated the production of geopolymer bricks through the activation of circulating fluidized bed combustion bottom ash through the use of 10 M LiOH·H$_2$O as an alkaline activator [26]. A compressive strength of 9.4 MPa was achieved after curing at a temperature of 40 °C for 7 days. In comparison to those test results, the compressive strength of the optimal geopolymer mixture 7 (30 ± 2 MPa) is about three times higher, which is mainly due to the difference in the precursors used and the chemical parameters of the alkali activators. Another recent study investigated the cold sintering process of MGS-1, which also led to a promising compressive strength result of 45 MPa [54]. Xiao et al. (2023) studied the additive manufacturing of high-solid-content lunar regolith simulant paste based on vat photopolymerization and the effect of water addition on the paste's retention properties. During that study, high-precision porous structures as well as integral one-piece movable parts were successfully fabricated, with compressive strengths of up to 444 MPa [55].

4.3. FTIR Analysis

The FTIR results for both the raw materials (Figure 10) and the geopolymer mixtures (Figure 11) enable the identification of the chemical bonds formed during the geopolymerization process. After geopolymerization, typical peaks were observed at wavenumbers of 970–1020 cm^{-1}, which are related to bending vibrations of Si-O-T (T = Si or Al), or asymmetric stretching vibrations. Those peaks can be related to the initial observed peak at a wavenumber of 1008 cm^{-1} in the geopolymer precursor MGS-1. The biggest difference

between the FTIR spectrum of geopolymer mixture 1 and those of mixtures 2 and 3 is the less pronounced peak at a wavenumber of 1440 cm^{-1}. This indicates that the C-O stretching vibrations from carbonate were present, to a lesser extent, in the geopolymers made with LiOH·H$_2$O as an alkali activator. The presence of carbon–oxygen bonds can affect the setting time and porosity of geopolymers and other cementitious materials. Polymerization or cross-linking reactions are influenced by C-O bonds in the matrix. A material with a higher number of carbon–oxygen bonds has a higher reactivity and thus a shorter setting time [56]. With regard to the porosity of the geopolymer matrix, carbon–oxygen bonds can influence chain packing and intermolecular reactions. Materials with higher numbers of cross-linked carbon–oxygen bonds tend to have a reduced free volume and higher density due to a denser packing of molecules [57]. The less pronounced C-O stretching vibrations in geopolymer mixtures 2 and 3 likely indicate a lower concentration of carbon–oxygen bonds, suggesting shorter setting times and higher porosity due to reduced reactivity and looser molecular packing [58]. Due to curing at 70 °C, early-age reactions are accelerated and result in higher porosity. Porosity is not only determined by the carbon–oxygen bonds themselves but also depends on other factors such as the chemical composition, the presence of catalysts or additives, the processing conditions, and the specific reactions occurring in the geopolymer [59]. Due to their shorter setting time, geopolymers with a combination of LiOH·H$_2$O and NaOH as alkali activators are expected to show a higher early-age compressive strength in comparison to those with NaOH [60].

The peaks at wavenumbers of 1416 cm^{-1} (Figure 11b) and 1422–1425 cm^{-1} (Figure 11c) indicate the C-O stretching vibrations from carbonate in the geopolymer matrix. During the geopolymerization process, metakaolin undergoes chemical reactions with alkaline activators, leading to the formation of a three-dimensional aluminosilicate network. The presence of C-O bonds can arise from organic impurities within the metakaolin. It can be concluded that geopolymer mixture 4 possessed the highest number of -OH groups and Si-O-Si bonds in all the tested geopolymers, including those with LiOH·H$_2$O as alkaline activators, based on the FTIR patterns.

4.4. Strength–Microstructure Relations in Geopolymers

To gain insights into the observed compressive strength variations among the different geopolymers studied in this research, the porosity of the hardened geopolymer pastes was examined using scanning electron microscopy (SEM). The SEM image of geopolymer mixture 1, characterized by a relatively low compressive strength of 5.8 MPa after 28 days of curing, reveals a porous structure with significant voids in the geopolymer matrix (Figure 12a). The abundance of pores is directly correlated with the low compressive strength observed in this mixture.

Comparing the SEM images of geopolymer mixtures 2 and 3, it becomes evident that geopolymer mixture 2 displays a rougher surface texture but with fewer voids compared to mixture 3 (Figure 12b,c). These observations suggest that the compressive strength of mixture 2 is higher than that of mixture 3, aligning with the measured compressive strength results (Figure 9a). A further analysis of the SEM images for geopolymer mixtures 6 and 7 revealed relatively dense structures with limited large pores (Figure 12d,e), akin to the structure observed in mixture 2 (Figure 12b). This elucidates why geopolymer mixtures 6 and 7 exhibit comparable compressive strength to mixture 2. These findings underscore the crucial relationship between microstructure and compressive strength in geopolymers, where variations in porosity directly impact material strength. A denser microstructure with fewer voids generally correlates with a higher compressive strength, highlighting the importance of optimizing mixture composition and processing conditions to achieve the desired material properties.

4.5. XRD Analysis

The XRD analysis results reveal that aluminosilicate amorphous materials are present in the geopolymer materials due to the geopolymerization process. The primary amorphous

mineral in the geopolymers is the aluminosilicate gel phase, which is formed through the reaction of aluminate and silicate and plays a critical role in binding the solid particles. Silica and alumina gels are other amorphous materials formed by the chemical reaction of soluble silicate species in alkaline media [61]. These gels contribute to the compressive strength development and thermal stability of geopolymers. The XRD patterns of the sodium- and lithium-based geopolymer samples manufactured in this paper are shown in Figure 12. The peak intensity of the crystalline materials decreased for geopolymer mixture 1. Since this geopolymer consists of only NaOH and Na_2SiO_3 as the alkali activators, a limited amount of amorphous aluminosilicate gels are formed since $LiOH·H_2O$ supports the formation of those gels. The other geopolymer mixture that used a combination of $LiOH·H_2O$ and NaOH as alkaline activators showed more intense peaks (Figure 13).
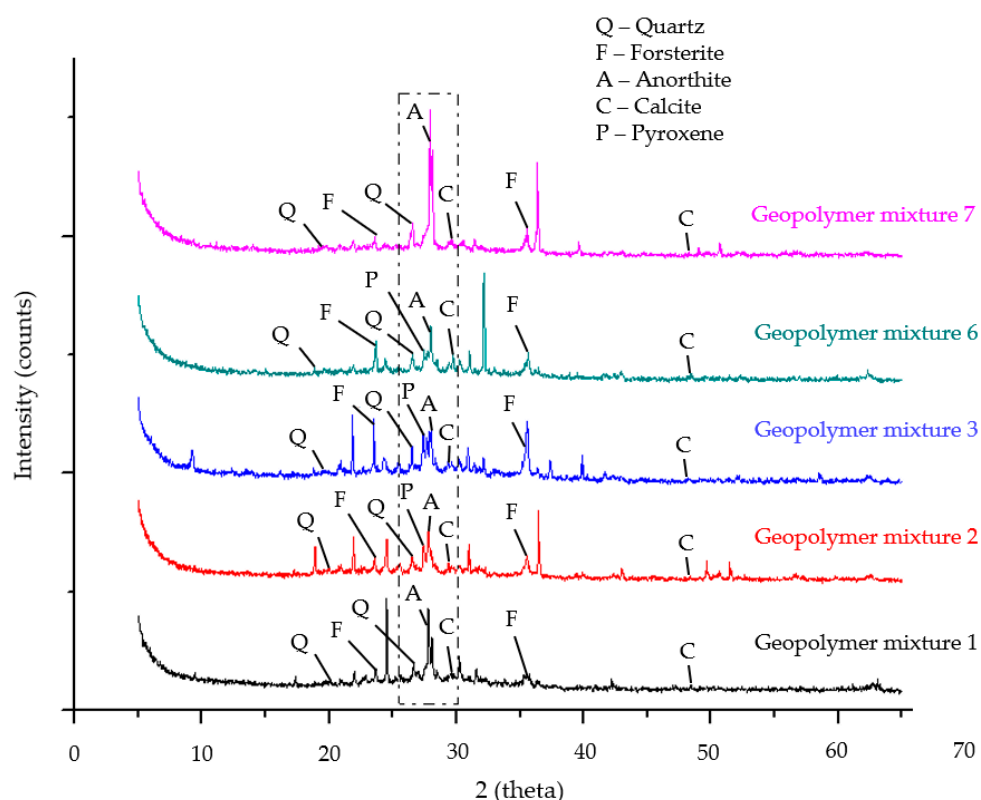

Figure 13. XRD patterns of geopolymer mixtures 1, 2, 3, 6 and 7.

Quartz (Q) is a common mineral in geopolymers, which can positively influence the compressive strength and durability aspects of the materials [62]. This mineral belongs to the group of tectosilicates and has a well-defined crystal structure. It can be considered a slowly reacting agent in the alkaline environment and acts as a filler. This mineral showed its main peaks for all the geopolymer mixtures at two-theta angles of 29.5° and 47.6°.

Forsterite (F) is a magnesium-silicate-rich member of the olivine mineral series. The olivine mineral represents 13.7 wt% of the total mineral composition of the raw MGS-1 regolith material. After the geopolymerization of the MGS-1 regolith, intensity peaks were observed at two-theta angles of 23° and 35.8°. Since forsterite is composed of silicon, magnesium and oxygen, it possesses the primary requirements for the formation of an aluminosilicate matrix.

Calcite (C) is another common mineral for all the geopolymer mixtures in this study. This mineral, composed of calcium carbonate, has both positive and negative effects on geopolymers' properties [63]. Calcite can act as a filler, improving the density and mechanical strength of the material. However, it can also reduce the chemical stability and

durability of geopolymers, particularly in acidic or aggressive environments. The main peaks for this mineral are observed at two-theta angles of 29.5° and 47.6°.

Anorthite (A) and pyroxene (P) were observed in the geopolymer mixtures, as they show their main peaks at two-theta angles within a range of 27–28°. Both minerals were also identified in the raw geopolymer precursor, MGS-1 [29]. These minerals act as reactive components in the geopolymerization process due to their silicate structures [64]. These structures participate in the formation of the aluminosilicate gel network characteristic of geopolymers. Moreover, their crystalline nature enhances the mechanical properties of the geopolymer matrix. Anorthite and pyroxene can improve compressive strength, flexural strength and resistance to abrasion and deformation [65]. Acting as nucleation sites, they facilitate the growth of the geopolymer gel network, resulting in a more densely packed and mechanically robust structure.

The XRD results suggest that a combination of $LiOH \cdot H_2O$ with $NaOH$ in the alkali activators performs better than $NaOH$ alone in improving the compressive strength of the geopolymers because the presence of $LiOH \cdot H_2O$ contributes to the formation of a more stable aluminosilicate gel phase. This gel phase acts as a binder, enhancing the interparticle bonding within the geopolymer matrix. A combined use of $LiOH \cdot H_2O$ and $NaOH$ might promote better reactivity and polymerization, leading to the development of a denser microstructure, which ultimately results in a higher compressive strength.

5. Conclusions

This paper presents a laboratory study on the feasibility of making high-strength geopolymer mixtures using the Martian regolith simulant MGS-1 as a precursor for possible building and infrastructure projects on Mars in the future. Various alkaline activators, such as sodium hydroxide ($NaOH$), lithium hydroxide ($LiOH \cdot H_2O$) and sodium silicate (Na_2SiO_3), were employed to investigate their efficiency in activating the precursor and compressive strength of the synthesized geopolymers. The influence of different factors, which include the milling of MGS-1, the alkali type and the concentration, on the performance of the synthesized geopolymers was examined. Based on the test results, the following conclusions can be drawn within the scope of this study:

- Geopolymers with the Martian regolith simulant MGS-1 as a precursor and $NaOH$ and Na_2SiO_3 as alkaline activator solutions have only very low compressive strength. A combined use of $LiOH \cdot H_2O$, $NaOH$ and Na_2SiO_3 as an alkaline activator solution led to a significant increase in the compressive strength of the geopolymers.
- Geopolymer mixtures 2–7 prepared with a combined lithium hydroxide and sodium silicate solution achieved compressive strengths of up to 30 MPa at a curing age of 7 d.
- The most optimal geopolymer mixture from this research was prepared with 8 M $LiOH \cdot H_2O$ + 1.5 M $NaOH$ and 11.6 wt% Na_2SiO_3 and showed a 7 d compressive strength of 30 ± 2 MPa.
- The FTIR spectra confirm successful geopolymerization based on the peaks at 970–1220 cm^{-1}, which are related to Si-O-Si stretching vibrations. This indicates the formation of silicate tetrahedral structures, which are crucial for the formation of the geopolymer network.
- The results from the SEM analysis explain the high compressive strength of some geopolymers, which is caused by a dense geopolymer structure, resulting in higher internal friction and interlocking with limited pore space.
- Other strength and durability properties of the developed geopolymers should be investigated to further evaluate their feasibility as suitable materials for building and infrastructure projects.

This study successfully demonstrates the production of higher-strength geopolymers compared to previous studies through the combined use of $LiOH \cdot H_2O$, $NaOH$ and Na_2SiO_3 as alkali activators. Hence, these results provide a basis for further research on the development of building materials with improved mechanical properties and better resistance to cosmic radiation needed for the environment on Mars.

References

1. Nazari-Sharabian, M.; Aghababaei, M.; Karakouzian, M.; Karami, M. Water on Mars—A literature review. *Galaxies* **2020**, *8*, 40. [CrossRef]
2. Banfield, D.; Spiga, A.; Newman, C.; Forget, F.; Lemmon, M.; Lorenz, R.; Murdoch, N.; Viudez-Moreiras, D.; Pla-Garcia, J.; Garcia, R.F.; et al. The atmosphere of Mars as observed by InSight. *Nat. Geosci.* **2020**, *13*, 190–198. [CrossRef]
3. Javaherikhah, A.; Valiente Lopez, M. Effective Factors for Implementing Building Information Modeling Using Fuzzy Method to Manage Buildings on Mars. *Buildings* **2023**, *13*, 2991. [CrossRef]
4. Hecht, M.; Hoffman, J.; Rapp, D.; McClean, J.; SooHoo, J.; Schaefer, R.; Aboobaker, A.; Mellstrom, J.; Hartvigsen, J.; Meyen, F.; et al. Mars Oxygen ISRU Experiment (MOXIE). *Space Sci. Rev.* **2021**, *217*, 9. [CrossRef]
5. Reidt, U.; Helwig, A.; Plobner, L.; Lugmayr, V.; Treutlein, U.; Kharin, S.; Smirnov, Y.; Novikova, N.; Lenic, J.; Fetter, V.; et al. Study of Initial Colonization by Environmental Microorganisms in the Russian Segment of the International Space Station (ISS). *Gravitational Space Res.* **2014**, *2*, 46–57. [CrossRef]
6. Golitsyn, G.S. *Estimates of Boundary Layer Parameters in Planetary Atmospheres of the Terrestrial Group*; NASA Goddard Space Flight Center: Greenbelt, MD, USA, 1969.
7. Certini, G.; Karunatillake, S.; Zhao, Y.-Y.S.; Meslin, P.-Y.; Cousin, A.; Hood, D.R.; Scalenghe, R. Disambiguating the soils of Mars. *Planet. Space Sci.* **2020**, *186*, 104922. [CrossRef]
8. Davis, J.; Balme, M.; Grindrod, P.; Williams, R.; Gupta, S. Extensive Noachian fluvial systems in Arabia Terra: Implications for early Martian climate. *Geology* **2016**, *44*, 847–850. [CrossRef]
9. Leovy, C. Weather and Climate on Mars. 2001. Available online: www.nature.com (accessed on 18 July 2023).
10. Liu, J.; Li, H.; Sun, L.; Guo, Z.; Harvey, J.; Tang, Q.; Lu, H.; Jia, M. In-situ resources for infrastructure construction on Mars: A review. *Int. J. Transp. Sci. Technol.* **2022**, *11*, 1–16. [CrossRef]
11. Kass, D.M.; Schofield, J.T.; Kleinböhl, A.; McCleese, D.J.; Heavens, N.G.; Shirley, J.H.; Steele, L.J. Mars Climate Sounder Observation of Mars' 2018 Global Dust Storm. *Geophys. Res. Lett.* **2020**, *47*, e2019GL083931. [CrossRef]
12. Dobrijevic, M.; Bertrix, I. Les Satellites de Jupiter et la Troisième loi de Kepler. 2022. Available online: https://www.researchgate.net/publication/359482126_Les_satellites_de_Jupiter_et_la_troisieme_loi_de_Kepler?channe (accessed on 20 March 2024).
13. Chen, C.; Habert, G.; Bouzidi, Y.; Jullien, A. Environmental impact of cement production: Detail of the different processes and cement plant variability evaluation. *J. Clean. Prod.* **2010**, *18*, 478–485. [CrossRef]
14. Davidovits, J. Synthetic Mineral Polymer Compound of the Silicoaluminates Family and Preparation Process. U.S. Patent 4472199A, 18 September 1984.
15. Davidovits, J. Mineral Polymers and Methods of Making Them. U.S. Patent US4349386A, 14 September 1982.
16. Davidovits, J. Properties of Geopolymer Cements. Available online: www.geopolymer.org (accessed on 20 July 2023).
17. Lingyu, T.; Dongpo, H.; Jianing, Z.; Hongguang, W. Durability of geopolymers and geopolymer concretes: A review. *Rev. Adv. Mater. Sci.* **2021**, *60*, 1–14. [CrossRef]
18. Alexiadis, A.; Alberini, F.; Meyer, M.E. Geopolymers from lunar and Martian soil simulants. *Adv. Space Res.* **2017**, *59*, 490–495. [CrossRef]
19. Chakraborty, S. Geopolymerization of Simulated Martian Soil. Master's Thesis, Tennessee Tech University, Cookeville, TN, USA, 2019. [CrossRef]
20. Ma, S.; Fu, S.; Wang, Q.; Xu, L.; He, P.; Sun, C.; Duan, X.; Zhang, Z.; Jia, D.; Zhou, Y. 3D Printing of Damage-tolerant Martian Regolith Simulant-based Geopolymer Composites. *Addit. Manuf.* **2022**, *58*, 103025. [CrossRef]

21. Golombek, M.; Warner, N.H.; Grant, J.A.; Hauber, E.; Ansan, V.; Weitz, C.M.; Williams, N.; Charalambous, C.; Wilson, S.A.; DeMott, A.; et al. Geology of the InSight landing site on Mars. *Nat. Commun.* **2020**, *11*, 1014. [CrossRef] [PubMed]
22. Jones, J.-P.; Jones, S.C.; Billings, K.J.; Pasalic, J.; Bugga, R.V.; Krause, F.C.; Smart, M.C.; Brandon, E.J. Radiation effects on lithium CFX batteries for future spacecraft and landers. *J. Power Sources* **2020**, *471*, 228464. [CrossRef]
23. Saleh, E.E.; Algradee, M.A.; El-Fiki, S.; Youssef, G. Fabrication of novel lithium lead bismuth borate glasses for nuclear radiation shielding. *Radiat. Phys. Chem.* **2022**, *193*, 109939. [CrossRef]
24. Askarian, M.; Tao, Z.; Samali, B.; Adam, G.; Shuaibu, R. Mix composition and characterisation of one-part geopolymers with different activators. *Constr. Build. Mater.* **2019**, *225*, 526–537. [CrossRef]
25. Durand-Manterola, H.J. Lithium generated by cosmic rays Lithium generated by cosmic rays: An estimator of the time that Mars had a thicker atmosphere and liquid water. *arXiv* **2012**, arXiv:1208.6311.
26. Chen, C.; Li, Q.; Shen, L.; Zhai, J. Feasibility of manufacturing geopolymer bricks using circulating fluidized bed combustion bottom ash. *Environ. Technol.* **2012**, *33*, 1313–1321. [CrossRef]
27. Tchakoute Kouamo, H.; Elimbi, A.; Mbey, J.; Sabouang, C.N.; Njopwouo, D. The effect of adding alumina-oxide to metakaolin and volcanic ash on geopolymer products: A comparative study. *Constr. Build. Mater.* **2012**, *35*, 960–969. [CrossRef]
28. Sarraf-Mamoory, R.; Demopoulos, G.P.; Drew, R.A.L. Preparation of fine copper powders from organic media by reaction with hydrogen under pressure: Part II. The kinetics of particle nucleation, growth, and dispersion. *Met. Mater. Trans. B* **1996**, *27*, 585–594. [CrossRef]
29. Cannon, K.M.; Britt, D.T.; Smith, T.M.; Fritsche, R.F.; Batcheldor, D. Mars global simulant MGS-1: A Rocknest-based open standard for basaltic martian regolith simulants. *Icarus* **2019**, *317*, 470–478. [CrossRef]
30. MacKenzie, K.J.D.; Brown, I.W.M.; Meinhold, R.H.; Bowden, M.E. Outstanding Problems in the Kaolinite-Mullite Reaction Sequence Investigated by 29Si and 27Al Solid-state Nuclear Magnetic Resonance: I, Metakaolinite. *J. Am. Ceram. Soc.* **1985**, *68*, 293–297. [CrossRef]
31. Karym, H.; Chbihi, M.E.M.; Benmokhtar, S.; Belaaouad, S.; Moutaabbid, M. Caracterisation of the Kaolinite Clay Minerals (Nador-North Morocco) Using Infrared Spectroscopy and Calorimetry of Dissolution. *Int. J. Recent Sci. Res.* **2015**, *6*, 4444–4448.
32. Tan, J.; Cai, J.; Li, J. Recycling of unseparated construction and demolition waste (UCDW) through geopolymer technology. *Constr. Build. Mater.* **2022**, *341*, 127771. [CrossRef]
33. Montes, C.; Broussard, K.; Gongre, M.; Simicevic, N.; Mejia, J.; Tham, J.; Allouche, E.; Davis, G. Evaluation of lunar regolith geopolymer binder as a radioactive shielding material for space exploration applications. *Adv. Space Res.* **2015**, *56*, 1212–1221. [CrossRef]
34. Lumley, J.S. The ASR expansion of concrete prisms made from cements partially replaced by ground granulated blastfurnace slag. *Constr. Build. Mater.* **1993**, *7*, 95–99. [CrossRef]
35. Duxson, P.; Provis, J.L. Designing precursors for geopolymer cements. *J. Am. Ceram. Soc.* **2008**, *91*, 3864–3869. [CrossRef]
36. Rovnaník, P. Effect of curing temperature on the development of hard structure of metakaolin-based geopolymer. *Constr. Build. Mater.* **2010**, *24*, 1176–1183. [CrossRef]
37. Puligilla, S.; Mondal, P. Co-existence of aluminosilicate and calcium silicate gel characterized through selective dissolution and FTIR spectral subtraction. *Cem. Concr. Res.* **2015**, *70*, 39–49. [CrossRef]
38. *T. S. EN. 196-1*; Methods of Testing Cement–Part 1: Determination of Strength. European Committee for Standardization: Brussels, Belgium, 2005; Volume 26.
39. Tian, Q.; Nordman, D.J.; Meeker, W.Q. Methods to Compute Prediction Intervals: A Review and New Results. *Stat. Sci.* **2022**, *37*, 580–597. [CrossRef]
40. Macário, I.P.E.; Veloso, T.; Frankenbach, S.; Serôdio, J.; Passos, H.; Sousa, C.; Gonçalves, F.J.M.; Ventura, S.P.M.; Pereira, J.L. Cyanobacteria as Candidates to Support Mars Colonization: Growth and Biofertilization Potential Using Mars Regolith as a Resource. *Front. Microbiol.* **2022**, *13*, 840098. [CrossRef] [PubMed]
41. Dong, R.; Tian, J.; Huang, Z.; Yu, Q.; Xie, J.; Li, B.; Li, C.; Chen, Y. Intermolecular binding of blueberry anthocyanins with water-soluble polysaccharides: Enhancing their thermostability and antioxidant abilities. *Food Chem.* **2023**, *410*, 135375. [CrossRef] [PubMed]
42. Kumaravel, S.; Girija, K. Development of High-Strength Geopolymer Concrete. 2014, pp. 8–13. Available online: www.stmjournals.com (accessed on 23 July 2023).
43. Caballero, L.R.; Paiva, M.d.D.M.; Fairbairn, E.d.M.R.; Filho, R.D.T. Thermal, mechanical and microstructural analysis of metakaolin based geopolymers. *Mater. Res.* **2019**, *22*, e20180716. [CrossRef]
44. Ayeni, O.; Onwualu, A.P.; Boakye, E. Characterization and mechanical performance of metakaolin-based geopolymer for sustainable building applications. *Constr. Build. Mater.* **2021**, *272*, 121938. [CrossRef]
45. Madavarapu, S.B.; Neithalath, N.; Rajan, S.; Marzke, R. FTIR Analysis of Alkali Activated Slag and Fly Ash Using Deconvolution Techniques. Master's Thesis, Arizona State University, Tempe, AZ, USA, 2014.
46. Aredes, F.; Campos, T.; Machado, J.; Sakane, K.; Thim, G.; Brunelli, D. Effect of cure temperature on the formation of metakaolinite-based geopolymer. *Ceram. Int.* **2015**, *41*, 7302–7311. [CrossRef]
47. He, P.; Wang, M.; Fu, S.; Jia, D.; Yan, S.; Yuan, J.; Xu, J.; Wang, P.; Zhou, Y. Effects of Si/Al ratio on the structure and properties of metakaolin based geopolymer. *Ceram. Int.* **2016**, *42*, 14416–14422. [CrossRef]

48. Albidah, A.; Alghannam, M.; Abbas, H.; Almusallam, T.; Al-Salloum, Y. Characteristics of metakaolin-based geopolymer concrete for different mix design parameters. *J. Mater. Res. Technol.* **2021**, *10*, 84–98. [CrossRef]

49. Davidovits, J. Geopolymers: Inorganic polymeric new materials. *J. Therm. Anal. Calorim.* **1991**, *37*, 1633–1656. [CrossRef]

50. Sohn, H.Y.; Moreland, C. The effect of particle size distribution on packing density. *Can. J. Chem. Eng.* **1968**, *46*, 162–167. [CrossRef]

51. Shakrani, S.A.; Ayob, A.; Ab Rahim, M.A.; Alias, S. Effect of Calcination Processes on the Crystallite Size, Grain Size and Particle Size of Water-Washed Kaolin Particles. *IOP Conf. Ser. Earth Environ. Sci.* **2024**, *1303*, 012006. [CrossRef]

52. McConville, C. Thermal Transformations in Kaolinite Clay Minerals. *Ceram. Eng. Sci. Proc.* **2008**, *22*, 149–160. [CrossRef]

53. Pavlova, A.; Trinh, T.T.; van Santen, R.A.; Meijer, E.J. Clarifying the role of sodium in the silica oligomerization reaction. *Phys. Chem. Chem. Phys.* **2013**, *15*, 1123–1129. [CrossRef]

54. Karacasulu, L.; Karl, D.; Gurlo, A.; Vakifahmetoglu, C. Cold sintering as a promising ISRU technique: A case study of Mars regolith simulant. *Icarus* **2023**, *389*, 115270. [CrossRef]

55. Xiao, C.; Zheng, K.; Chen, S.; Li, N.; Shang, X.; Wang, F.; Liang, J.; Khan, S.B.; Shen, Y.; Lu, B.; et al. Additive manufacturing of high solid content lunar regolith simulant paste based on vat photopolymerization and the effect of water addition on paste retention properties. *Addit. Manuf.* **2023**, *71*, 103607. [CrossRef]

56. Rakhimova, N.R.; Rakhimov, R.Z. Reaction products, structure and properties of alkali-activated metakaolin cements incorporated with supplementary materials—A review. *J. Mater. Res. Technol.* **2019**, *8*, 1522–1531. [CrossRef]

57. Duxson, P.; Provis, J.L.; Lukey, G.C.; Mallicoat, S.W.; Kriven, W.M.; van Deventer, J.S.J. Understanding the relationship between geopolymer composition, microstructure and mechanical properties. *Colloids Surf. A Physicochem. Eng. Asp.* **2005**, *269*, 47–58. [CrossRef]

58. Wan-En, O.; Yun-Ming, L.; Li-Ngee, H.; Abdullah, M.M.A.B.; Shee-Ween, O. The Effect of Sodium Carbonate on the Fresh and Hardened Properties of Fly Ash-Based One-Part Geopolymer. In *IOP Conference Series: Materials Science and Engineering*; IOP Publishing Ltd.: Bristol, UK, 2020. [CrossRef]

59. Zhang, X.; Bai, C.; Qiao, Y.; Wang, X.; Jia, D.; Li, H.; Colombo, P. Porous geopolymer composites: A review. *Compos. Part A Appl. Sci. Manuf.* **2021**, *150*, 106629. [CrossRef]

60. Gurvich, L.V.; Bergman, G.A.; Gorokhov, L.N.; Iorish, V.S.; Leonidov, V.Y.; Yungman, V.S. Thermodynamic properties of alkali metal hydroxides. Part 1. Lithium and sodium hydroxides. *J. Phys. Chem. Ref. Data* **1996**, *25*, 1211–1276. [CrossRef]

61. Hajimohammadi, A.; Provis, J.L.; van Deventer, J.S.J. Effect of alumina release rate on the mechanism of geopolymer gel formation. *Chem. Mater.* **2010**, *22*, 5199–5208. [CrossRef]

62. Song, M.; Jiaping, L.; Qian, J.; Jianzhong, L.; Liang, S. Experimental Study on Utilization of Quartz Mill Tailings as a Filler to Prepare Geopolymer. *Miner. Process. Extr. Met. Rev.* **2016**, *37*, 311–322. [CrossRef]

63. Sauffi, A.S.; Ibrahim, W.M.W.; Abdulla, M.M.A.B.; Ahmad, R.; Zaidi, F.A.; Sandu, A.V. A Review of Carbonate Minerals as an Additive to Geopolymer Materials. In *IOP Conference Series: Materials Science and Engineering*; Institute of Physics Publishing: Bristol, UK, 2019. [CrossRef]

64. Yip, C.K.; Lukey, G.C.; Provis, J.L.; van Deventer, J.S. Effect of calcium silicate sources on geopolymerisation. *Cem. Concr. Res.* **2008**, *38*, 554–564. [CrossRef]

65. Klyuev, A.; Kashapov, N.; Klyuev, S.; Ageeva, M.; Fomina, E.; Sabitov, L.; Nedoseko, I.; Vatin, N.I.; Kozlov, P.; Vavrenyuk, S. Alkali-activated binders based on technogenic fibrous waste. *Case Stud. Constr. Mater.* **2023**, *18*, e02202. [CrossRef]